Inorganic Chemistry

ARTICLE

pubs.acs.org/IC

In Vitro Imaging and Human Serum Albumin Responsive Dimeric Lanthanide DO3A Complex

Yuen On Fung,[†] Wanqing Wu,[⊥] Chi-Tung Yeung,[†] Hoi-Kuan Kong,[‡] Kenny Kam-Cheng Wong,[§] Wai-Sum Lo,[†] Ga-Lai Law,[§] Ka-Leung Wong,[‡] Chi-Kong Lau,[∥] Chi-Sing Lee,[⊥] and Wing-Tak Wong*[,†]

[†]Department of Applied Biology and Chemical Technology, Hong Kong Polytechnic University, Hung Hom, Kowloon, Hong Kong SAR

[‡]Department of Chemistry, Hong Kong Baptist University, Kowloon Tong, Hong Kong SAR

[§]Department of Chemistry, The University of Hong Kong, Pokfulam, Hong Kong SAR

[∥]School of Biomedical Sciences, The Chinese University of Hong Kong, Shatin, New Territories, Hong Kong SAR

[⊥]Laboratory of Chemical Genomics, School of Chemical Biology and Biotechnology, Peking University Shenzhen Graduate School, Shenzhen University Town, Xili, Shenzhen 518055, China

Supporting Information

ABSTRACT:

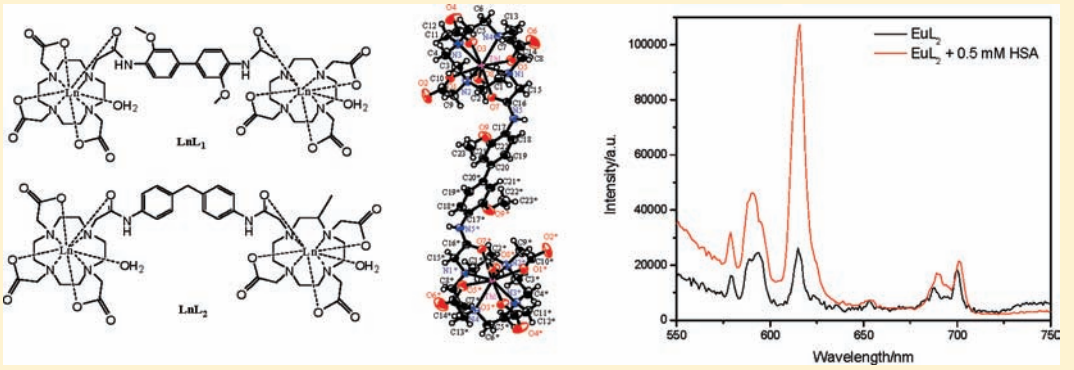

Two series of dimeric DO3A (1,4,7,10-tetraazacyclodecane-1,4,7-triacetate) lanthanide complexes (Ln$\mathbf{L_1}$−Ln$\mathbf{L_2}$, Ln = Eu, Gd, and Tb) have been synthesized with two different bridged chromophores. The X-ray structures of dimeric Ln$\mathbf{L_1}$ (Ln = Gd and Tb) complexes show that each metal ion has nine coordination numbers with eight directly bound donor atoms of the ligand and one oxygen donor from the water molecule. Photophysical measurements indicate that the bridged antenna in Ln$\mathbf{L_2}$ gives a higher efficiency than that of Ln$\mathbf{L_1}$ and is responsive to the protein Human Serum Albumin (HSA), giving an f−f luminescence signal enhancement with a binding constant log K = 4.84. *In vitro* imaging of Eu$\mathbf{L_1}$ and Eu$\mathbf{L_2}$ in HeLa cells has been recorded, and Eu$\mathbf{L_2}$ has demonstrated a higher rate of cellular uptake and low cytotoxicity (IC_{50} = 3 mM).

INTRODUCTION

Luminescent lanthanide complexes are of increasing interest in photochemistry,[1−3] organic optoelectronics,[4−6] luminescence sensors,[7−11] and molecular imaging.[12−16] Lanthanide ions are attractive substitutes for the more commonly used organic fluorophores, as lanthanide complexes exhibit long-lived luminescence lifetimes, large Stokes shifts, and sharp emission peaks.[2,12] There are various examples of long-lived $4f^N$−$4f^N$ luminescence sensitized by the antenna effect following single or even multiphoton absorption of multidentate amide ligands.[17−21] These phenomena are particularly useful for addressing the issue of autofluorescence in confocal microscopy imaging and can be used as a high throughput screening method to detect low signal-to-noise biologically meaningful molecules (e.g., citrate) *in situ*.[15] In addition, applications take advantage of the intrinsic property of the trivalent lanthanide ions—hypersensitive emission to the coordination environment—for real-time responsive imaging as their emission signal changes with structural variations.

The past two decades have witnessed rapid development in the use of DO3A as templates to develop lanthanides for molecular imaging, medical diagnosis, and therapy.[15] The ease in which DO3A templates could be modified to develop lanthanide complexes along with excellent water-solubility and stability *in vitro*/*in vivo* are major reasons for the growing interest in

Received: January 11, 2011
Published: May 18, 2011

   dx.doi.org/10.1021/ic2004672 | *Inorg. Chem.* 2011, 50, 5517–5525

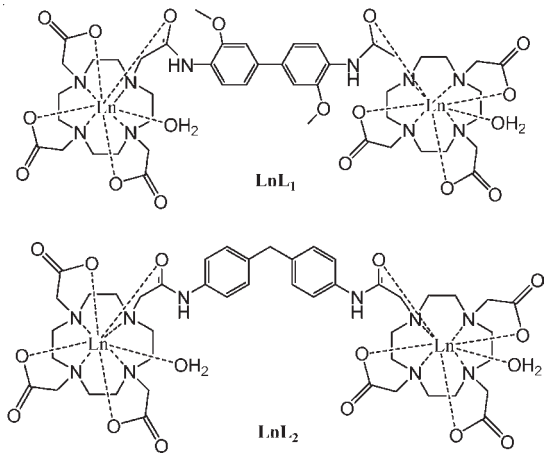

Figure 1. The molecular structures of Ln$\mathbf{L_1}$−Ln$\mathbf{L_2}$ (Ln = Eu and Tb).

them.[22−24] Demand for these complexes has increased due to current development in time-resolved imaging as the micro- to millisecond lifetimes of lanthanide ions make them ideal candidates for bioimaging.[20] There are numerous accounts on the use of DO3A to form monomeric lanthanide complexes in the literature,[15,16] but only a few dimeric lanthanide complexes with DO3A have been reported as having known molecular structures.[25−27] Shiraishi and his group have reported that dimeric lanthanide complexes of DO3A efficiently suppress intra- and intermolecular BET and show higher luminescence efficiency than monomeric lanthanide complexes of DO3A.[28] Costa has also reported that the dimeric cyclen-based marcocyclic lanthanide is more favorable than its monomeric unit in MRI contrast agents.[29,30] Recently, some DO3A-based dimeric lanthanide luminescent probes have been successfully developed for specific aliphatic dicarboxylates.[30] Our complexes (Gd$\mathbf{L_1}$ and Tb$\mathbf{L_1}$) are two of the few DO3A-based dimeric lanthanide complexes whose molecular structures have been fully studied.

The stability of these lanthanide complexes was examined with the titration of various biological molecules such as citrate, urate, and HSA. Ln$\mathbf{L_1}$ has a linear structure and did not show any enhancement of f−f luminescence when HSA was added. On the other hand, Ln$\mathbf{L_2}$ was responsive to HSA with a strong binding constant (log K = 4.84) and showed f−f luminescence enhancement, making it useful as a potential biosensor. Ln$\mathbf{L_2}$ consists of a spacer with two benzyl groups and a bent geometric shape similar to that of bisphenol A (BPA). BPA is an organic compound that can bind to various biological molecules such as proteins and DNA.[31−33] It has been recently reported that bisphenol A binds strongly and noncovalently to proteins.[33] Herein is the synthesis of the two series of nine-coordinated dimeric lanthanide complexes Ln$\mathbf{L_1}$ and Ln$\mathbf{L_2}$, where Ln = Gd, Eu, and Tb (Figure 1); the goal is to devise more biologically friendly materials with long emission lifetimes for time-resolved imaging. Their molecular structures, photophysical properties in solution, and protein-binding abilities were studied, and cellular-uptake experiments were performed.

EXPERIMENTAL SECTION

General Remarks. All reagents were purchased from commercial sources and used as received unless otherwise stated. *o*-Dianisidine, 4,4′-diaminodiphenylmethane, *tert*-butyl bromoacetate, 1,4,7,10-tetraaza-cyclododecane (cyclen), chloroacetyl chloride, 4,4′-diaminobenzanilide, trifluoroacetic acid, and 4-(chloromethyl)benzoyl chloride were from Sigma-Aldrich. Gadolinium carbonate, europium carbonate, europium chloride, terbium carbonate, terbium chloride, manganese chloride, and ytterbium chloride were purchased from Strem Chemicals, Inc. The solvents were used as received without further purification unless otherwise specified. Pyridine, triethylamine, and DMF were distillated over calcium hydride before use. ^{1}H and ^{13}C NMR spectra were recorded on DPX300 and AV400 Bruker FT-NMR spectrometers. Electrospray ionization mass spectra (ESI-MS) were acquired on a Finnigan MAT LCQ mass spectrometer. The triprotected cyclen (DO3A), tris-(*tert*-butoxycarbonylmethyl)-1,4,7,10-tetraazacyclododecane·HCl, was prepared according to a previously reported method.

General Procedure for Synthesis of the Dichlorodiamide-linkers, K. Chloroacetyl chloride (4 equiv) was added dropwise into the corresponding diamine (1 equiv) in 100 mL of H_2O containing NaOH (4 equiv). The reaction mixture was stirred overnight at room temperature under nitrogen.

N,N′-(3,3′-Dimethoxybiphenyl-4,4′-diyl)bis(2-chloroacetamide), ***K₁***. The procedure was followed using *o*-dianisidine (1 g, 4 mmol). The reaction was filtered to yield a brown solid (1.43 g, 90%). ^{1}H NMR (400 MHz, DMSO): δ/ppm 9.59 (2H, s), 8.11−8.08 (2H, d), 7.36 (2H, s), 7.32−7.30 (2H, d), 4.44 (4H, s), 3.99 (2H, s). ^{13}C NMR (400 MHz, DMSO): δ/ppm 164.2 (2 × C), 149.2 (2 × C), 136.0 (2 × C), 125.5 (2 × C),121.0 (2 × CH), 118.0 (2 × CH), 108.9 (2 × CH), 55.4 (2 × CH_3), 42.9 (2 × CH_2). ESI-MS, *m/z*: 398.2 $(M + H)^+$.

N,N′-(4,4′-Methylene-bis(1,4-phenylene))bis(2-chloroacetamide), ***K₂***. The procedure was followed using 4,4′-diaminodiphenylmethane (1 g, 5 mmol). A white solid was collected by filtration (1.32 g, 75%). ^{1}H NMR (400 MHz, Acetone): δ/ppm 9.36 (2H, s), 7.59−7.57 (4H, d), 7.22−7.17 (4H, d), 4.20 (4H, s), 3.92 (2H, s). ^{13}C NMR (400 MHz, DMSO): δ/ppm 164.0 (2 × C), 136.4 (2 × C), 136.0 (2 × C), 128.5 (4 × CH), 119.1 (4 × CH), 43.1 (2 × CH_2), 41.0 (C). ESI-MS *m/z*: 352.2 $(M + H)^+$.

General Procedure for Synthesis of the Bis(*t*-butyl-cyclen)-linkers, I. The dichlorodiamide-linker (**K**; 1 equiv) and DO3A (2.5 equiv) were added into MeCN (50 mL) with excess Na_2CO_3. The reaction mixture was stirred under nitrogen at 70−75 °C for 3 days. After cooling to room temperature, the solid was filtered, and the solvent was removed under reduced pressure. The product was purified with column chromatography on silica gel eluting with DCM/MeOH.

I₁. The general procedure was followed using $\mathbf{K_1}$ (0.2 g, 0.5 mmol) and DO3A (0.65 g, 1.26 mmol). The crude product was then separated by column chromatography on silica gel eluting with DCM/MeOH (97:3), yielding a yellow solid (0.37 g, 55%). ^{1}H NMR (400 MHz, $CDCl_3$): δ (ppm) 8.4 (2H, s), 8.19−8.17 (2H, d), 7.01 (2H, s), 6.97−6.95 (2H, d), 3.96 (6H, s), 3.09−2.17 (48H, br), 1.47−1.42 (54H, d). ^{13}C NMR (400 MHz, $CDCl_3$): δ (ppm) 172.6 (6 × C), 170.2 (2 × C), 149.0 (2 × C), 137.3 (2 × C), 126.5 (2 × C), 120.9 (2 × CH), 118.8 (2 × CH), 109.0 (2 × CH), 81.8 (6 × C), 57.3 (2 × CH_3), 55.9 (2 × CH_2), 55.7 (6 × CH_2), 52.5 (8 × CH_2), 48.6 (8 × CH_2), 27.9 (18 × CH_3). ESI-MS *m/z*: 699.4 $(M + H)^{2+}$.

I₂. The general procedure for the intermediates was followed with linker $\mathbf{K_2}$ (0.2 g, 0.5 mmol) and DO3A (0.73 g, 1.4 mmol). The crude product was separated by column chromatography on silica gel eluting with DCM/MeOH (95:5), yielding a yellow solid (0.35 g, 53%). ^{1}H NMR (300 MHz, $CDCl_3$): δ (ppm) 10.44 (2H, s), 7.83−7.80 (4H, d), 6.98−6.96 (4H, d), 3.81 (2H, s), 3.38−2.10 (48H, br), 1.46−1.41 (54H, d). ^{13}C NMR (400 MHz, $CDCl_3$): δ (ppm) 172.2 (6 × C), 170.6 (2 × C), 137.1 (2 × C), 136.0 (2 × C), 128.3 (4 × CH), 120.1 (4 × CH), 81.9 (6 × C), 56.7 (2 × CH_2), 55.6 (6 × CH_2), 52.5 (8 × CH_2), 47.6 (8 × CH_2), 27.8 (18 × CH_3). ESI-MS *m/z*: 676.4 $(M + H)^{2+}$.

General Procedure for Deprotection of (L_1 and L_2). TFA (20 mL) was added into $\mathbf{I_1}$ or $\mathbf{I_2}$ in DCM (25 mL). The solution was stirred overnight at ambient temperature. The solvent was removed under vacuum conditions, and the solid was washed with DCM (6 times).

***L*$_1$.** The procedure for synthesizing $\mathbf{L_1}$ was followed, and 0.37 g of $\mathbf{I_1}$ was used. A brown solid was yielded (0.33 g, 90%). ^{1}H NMR (400 MHz, D_2O): δ (ppm) 7.85 (2H, s), 7.14 (4H, s), 4.41−3.72 (16H, br), 3.61 (6H, s), 3.46−2.48 (32H, br). ^{13}C NMR (400 MHz, D_2O): δ (ppm) 174.8 (2 × C), 169.4 (4 × C), 164.1 (2 × C), 151.0 (2 × C), 121.8 (2 × C), 118.9 (2 × C), 116.0 (2 × CH), 113.3 (2 × CH), 109.9 (2 × CH), 72.2 (6 × C), 61.4 (2 × CH_3), 56.9 (2 × CH_2), 54.5 (2 × CH_2), 54.1 (2 × CH_2), 52.8 (4 × CH_2), 50.0 (4 × CH_2), 49.5 (4 × CH_2). ESI-MS m/z: 509.3 $(M + H)^{2+}$, 1017.5 $(M + H)^+$.

***L*$_2$.** The procedure for synthesizing $\mathbf{L_2}$ was followed, and 0.35 g of $\mathbf{I_2}$ was used. A brown solid was yielded (0.31 g, 90%). ^{1}H NMR (400 MHz, MeOD): δ (ppm) 7.50−7.48 (4H, d), 7.12−7.10 (4H, d), 3.93−3.88 (18H, br), 3.51−3.29 (32H, br). ^{13}C NMR (400 MHz, MeOD): δ (ppm) 174.7 (2 × C), 169.5 (4 × C), 162.7 (2 × C), 138.9 (2 × C), 137.3 (2 × C), 130.2 (4 × CH), 121.1 (4 × CH), 72.9 (6 × CH_2), 61.9 (2 × CH_2), 54.8 (8 × CH_2), 52.1 (8 × CH_2), 41.5 (CH_2). ESI-MS m/z: 486.5 $(M + H)^{2+}$, 971.7$(M + H)^+$.

General Procedure for the Synthesis of the Ln Complexes. $\mathbf{L_1}$ or $\mathbf{L_2}$ (0.2 g) and $Ln(CO_3)_3$ (0.1 g) were stirred in H_2O (40 mL) at 65 °C for 24 h. Any excess $Ln(CO_3)_3$ was filtered off, and the solvent was removed under vacuum conditions.

*Eu**L*$_1$ *(0.23 g, 90%).* ESI-MS m/z: 1329 $(M + H)^+$. Elemental Analysis: $C_{46}H_{62}N_{10}O_{16}Eu_2$ Calcd: C, 42.62; H, 4.75; N, 10.65. Found: C, 42.82; H, 4.60; N, 11.02.

*Gd**L*$_1$ *(0.23 g, 90%).* ESI-MS m/z: 1326 $(M + H)^+$. Elemental Analysis: $C_{46}H_{62}N_{10}O_{16}Gd_2$ Calcd: C, 41.68; H, 4.71; N, 10.57. Found: C, 41.65; H, 4.73; N, 10.52.

*Tb**L*$_1$ *(0.23 g, 90%).* ESI-MS m/z: 1329 $(M + H)^+$. Elemental Analysis: $C_{46}H_{62}N_{10}O_{16}Tb_2$ Calcd: C, 41.58; H, 4.70; N, 10.54. Found: C, 41.60; H, 4.71; N, 12.02.

*Eu**L*$_2$ *(0.22 g, 85%).* ESI-MS m/z: 1283 $(M + H)^+$. Elemental Analysis: $C_{45}H_{60}N_{10}O_{14}Eu_2$ Calcd: C, 42.13; H, 4.71; N, 10.92. Found: C, 42.56; H, 4.82; N, 11.12.

*Gd**L*$_2$ *(0.22 g, 85%).* ESI-MS m/z: 1280 $(M + H)^+$. Elemental Analysis: $C_{45}H_{60}N_{10}O_{14}Gd_2$ Calcd: C, 42.24; H, 4.73; N, 10.95. Found: C, 42.22; H, 4.69; N, 10.91.

*Tb**L*$_2$ *(0.22 g, 85%).* ESI-MS m/z: 1283 $(M + H)^+$. Elemental Analysis: $C_{45}H_{60}N_{10}O_{14}Tb_2$ Calcd: C, 42.59; H, 4.77; N, 11.04. Found: C, 42.72; H, 4.78; N, 11.21.

Spectroscopic and Photophysical Studies. UV−visible absorption spectra in the range of 200 to 1100 nm were recorded with a HP UV-8453 spectrophotometer. Single-photon luminescence and lifetime spectra were recorded using an Edinburgh Instrument FLS920 Combined Fluorescence Lifetime and Steady-State Spectrophotometer equipped with a single photon counting photomultiplier in a Peltier Cooled Housing (185−850 nm). The spectra were corrected for detector response and stray background light phosphorescence. The solution state quantum yields of the lanthanide complexes were measured with a Demountable 142 mm (inner)-diameter barium sulphide coated integrating sphere supplied with two access ports.

For the spectrofluorometric titrations, all of the solvents used were of analytical grade, and the water used was purified by double distillation. Measurements were taken after equilibrium was attained, and the $^5D_0 \rightarrow {}^7F_2$ emission (europium) was monitored. Luminescent responses in terms of $I_o/(I - I_o)$ were plotted as a function of analyte concentration. For the determination of binding strengths of the various analyte adducts, a series of analyte solutions at a known concentration were mixed with the anion solutions at various concentrations. The titration curve was then fitted either with the 1:1 or 1:2 Benesi−Hildebrand equations (below) to check whether it was a 1:1 or 1:2 donor−acceptor interaction. The 1:1 donor−acceptor interaction was analyzed by Benesi−Hildebrand equations for spectrofluorometric titration.

$$\frac{I_o}{I - I_o} = \left(\frac{a}{b - a}\right)\left(\frac{1}{K_B[\text{substrate}]} + 1\right)$$

The 1:2 donor−acceptor interaction was analyzed by Benesi−Hildebrand equations for spectrofluorometric titration.

$$\frac{I_o}{I - I_o} = \left(\frac{a}{b - a}\right)^2\left(\frac{1}{K_B[\text{substrate}]^2} + 1\right)$$

I_o and I are the luminescence intensity of the fluorogenic reagent in the absence and presence of the substrate, respectively, a and b are constants, and [substrate] is the concentration of the target analyte. The binding constants K_B were estimated from the ratio between the y intercept and the slope, which was obtained from the line of best fit by using Benesi−Hildebrand equations depending on the 1:1 or 1:2 host−guest interactions.[34]

SDS-Polyacrylamide Gel Electrophoresis Analysis. Amounts of HSA protein of decreasing concentrations (500 ng to 3.9 ng) were loaded into the 12% SDS-polyacrylamide gel with the protein marker (LMW-SDS Marker Kit, GE) and separated under a constant voltage of 200 V for 45 min. The gel was then fixed and stained with dye for 30 min and analyzed with a Typhoon Trio Imager (GE) with excitation and emission at 457 nm and ∼620 nm, respectively.[35]

The Cellular Uptake of Europium Complexes. To measure the intracellular concentration of the complex, 1 × 105 cells were plated in each well and incubated with the complex with different concentrations (0.01, 0.025, 0.05, 0.1, and 0.2 mM). After coincubation, the complex-containing cell culture medium was removed, and exposed cells were further washed with 1 × PBS 3 times to remove any complex adhering to the outer cell membrane. Then, the cells were harvested from the well plates using trypsin-EDTA and dispersed into 1.5 mL of the culture medium. The exposed cells were collected with a centrifuge, and the cell pellet was digested in 500 μL of concentrated HNO_3 at 70 °C for 4 h. The intracellular concentration of Eu was determined using an Agilent 7500 series of inductively coupled plasma mass spectroscopy (ICP-MS). All ICP experiments were performed in triplicate, and values obtained were averaged. The concentration of Eu per cell was calculated by determining the concentration of Eu in the cell lysate by ICP-MS and divided by the number of cells, which was counted using a hematocytometer.

Tissue Cultures and in Vitro Microscopy Imaging. Human cervical carcinoma (HeLa) cells were maintained in an RMPI 1640 medium supplemented with 10% fetal bovine serum (FBS) and 1% penicillin and streptomycin in 5% CO_2. Cells were passaged every 3−5 days. To study the in vitro behavior of the lanthanide complexes, experiments were carried out with a commercially available UV confocal microscope [Leica SP5 (upright configuration)] equipped with a xenon lamp. For the in vitro imaging, the cells were imaged in the tissue culture chamber (5% CO_2, 37 °C). The excitation beam was produced by the xenon lamp with a power of ∼6 to 10 mW and focused on coverslip-adherent cells using a 40× oil immersion or 60× water immersion objective. Long pass filter (LB500) was used. An MTT viability assay was performed, as reported in the previous literature. Briefly, 3000 HeLa cells were seeded in 96-well plates 24 h prior to exposure to the europium complex or DMSO as a control. After various exposure time points, 20 μL of MTT [3-(4,5-dimethylthiazol-2-yl)-2,5-diphenyltetrazolium bromide] solution (5 mg/mL) was added to the culture medium in each well and incubated for 5 h at 37 °C. The medium was removed, 200 μL of DMSO solubilizing reagent was added, and incubation was carried out for another hour to dissolve the formazan crystals. The absorbance was measured at 570 nm on a Labsystem Multiskan microplate reader (Merck Eurolab, Switzerland). MTT assays were

Scheme 1. Reaction Schemes of Dimeric Lanthanide Complexes (LnL_1–LnL_2, Ln = Eu, Tb, and Gd)[a]

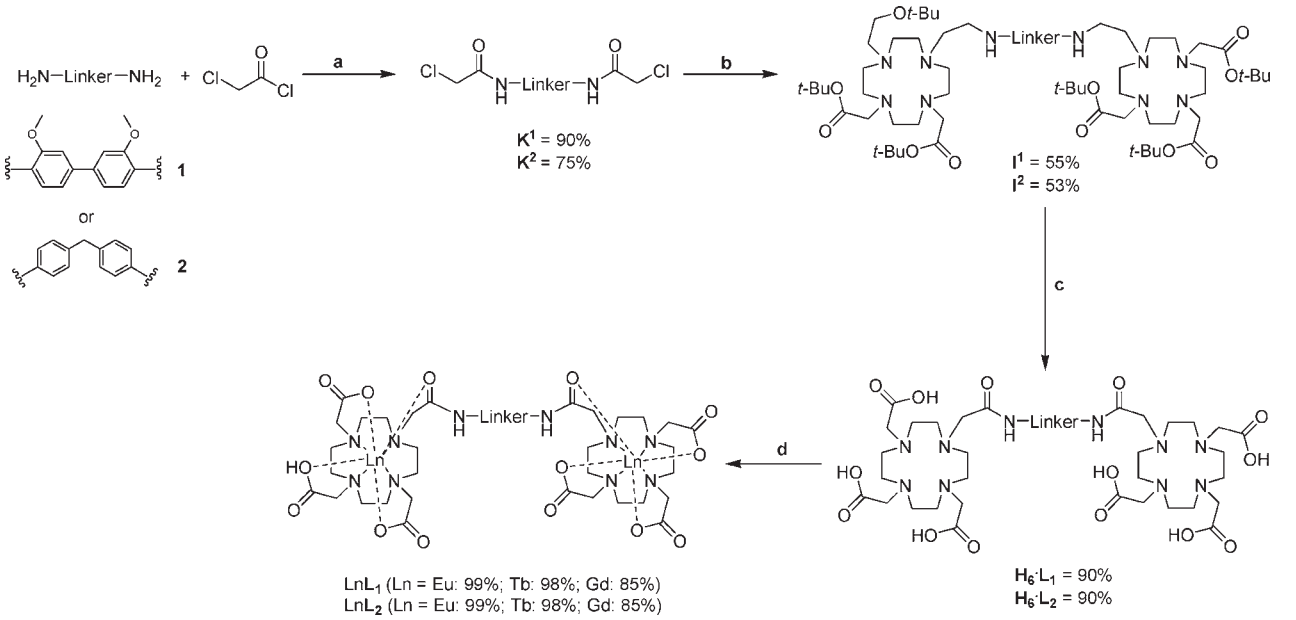

[a] Reagents and conditions. (a) $NaOH/H_2O$, r.t., 4 h; (b) 2.5 equiv triester-cyclen, Na_2CO_3/MeCN, 65–70 °C, 24 h; (c) (i) TFA/CH_2Cl_2, r.t., 12 h; (d) $Ln_2(CO_3)_3$, H_2O, 70–75 °C, 12 h.

conducted in triplicate wells and repeated twice. Each data point represents the ratio of mean values between the europium and the DMSO control.[36]

Crystallographic information is available as records CCDC 804789 and CCDC 804790 from The Cambridge Crystallographic Data Centre (CCDC). These data can be obtained free of charge from the CCDC via the Web link www.ccdc.cam.ac.uk/data_request/cif.

RESULTS AND DISCUSSION

a. Synthesis of Ligand H8·L_1 and H8·L_2 Solid State Structure of LnL_2 (Ln = Tb and Gd). The synthesis of the two ligands $\mathbf{L_1}$ and $\mathbf{L_2}$ and their corresponding lanthanide complexes is shown in Scheme 1. In the synthesis of H8·$\mathbf{L_1}$, the linker *o*-dianisidine 1 was first reacted with chloroacetyl chloride to afford the α-chlorodiamide intermediate $\mathbf{K_1}$ in high yield (90%). The key intermediate triester bis(cyclen) unit ($\mathbf{I_1}$) was obtained by treating $\mathbf{K_1}$ with tris-(*tert*-butoxycarbonylmethyl)-1,4,7,10-tetraazacyclododecane·HCl in the presence of excess Na_2CO_3 in CH_3CN for 3 days. $\mathbf{I_1}$ was then purified by flash column chromatography using CH_2Cl_2/CH_3OH as an eluent. Subsequent deprotection of $\mathbf{I_1}$ afforded the desired H8·$\mathbf{L^1}$ in good yield (90%). Synthesis of H8·$\mathbf{L_2}$ followed the same procedure with linker 4,4′-diaminodiphenylmethane. The two ligands were characterized by conventional methods.

The dimeric lanthanide complexes Ln$\mathbf{L_1}$ and Ln$\mathbf{L_2}$ (Ln = Eu or Gd) were formed out of the corresponding ligands by stirring the ligands with excess lanthanide carbonate salts [$Ln_2(CO_3)_3$, where Ln = Eu(III) and Gd(III)] in water at 65 °C for 24 h. All lanthanide complexes were isolated as colorless solids.

There are only a few dimeric DO3A lanthanide complexes that have been reported with their known molecular structures. Ln$\mathbf{L_1}$ (Ln = Gd and Tb) crystal structures were obtained by slow evaporation of the corresponding concentrated aqueous solutions. Table 1 shows the crystal data and structure refinement parameters for Gd$\mathbf{L_1}$ and Tb$\mathbf{L_1}$. Selected bond lengths (Å) and angles (deg) are given in Table 2. Figure 2 shows the molecular structure of a Tb$\mathbf{L_1}$ ($Tb_2(C_{46}H_{66}N_{10}O_{18})(H_2O)_2]\cdot 18(H_2O)\}$) unit and the crystal packing diagram of Tb$\mathbf{L_1}$ without solvated water molecules. Since the Tb$\mathbf{L_1}$ complex is symmetrical, the two terbium ions have identical coordination geometries. Each is nine-coordinated and has slightly distorted monocapped square antiprism geometry. This geometry is also commonly found in monomeric octadenate lanthanide cyclen complexes. The lanthanide ion is coordinated to four nitrogens of the cyclen ring as well as three amide oxygen atoms of the pendant arms, with a range of 2.308–2.385 Å for Ln–O bond and 2.631–2.685 Å for Ln–N, and there are two further Ln–O coordinations, arising from the aqua ligand and the amide that leads to the bridge, in which the Ln–O(amide) has a longer bond length than the other three (2.425 Å). The two phenyl rings of the linker that adopt the transoid geometry with two methoxy groups are found to be *trans* to each other. The two phenyl rings are found to be coplanar, with a torsion angle of 180.00°. The Tb–Tb distance between neighboring dimers is ca. 16.22 Å. Tb$\mathbf{L_1}$ and Gd$\mathbf{L_1}$ show similar structural data. To the best of our knowledge, these complexes are among the few DO3A-based dimeric lanthanide complexes that have full studies on their molecular structures.

b. Photophysical Properties of LnL_1 and LnL_2 (Ln = Eu, Tb, and Gd). The two series of dimeric lanthanide complexes were recrystallized in MeOH. Their photophysical properties in DMSO were then analyzed, and Table 3 summarizes the results. After complexation, the π to π^* absorption bands of Ln$\mathbf{L_1}$ and Ln$\mathbf{L_2}$ (Ln = Eu, Gd, and Tb) were red-shifted by 1000 cm^{-1} and 1500 cm^{-1}, respectively, and their molar extinction coefficients increased slightly from 3000 to ~5000 M^{-1} cm^{-1} (Table 3).

The $4f^N$ emission spectra of Tb$\mathbf{L_1}$ and Tb$\mathbf{L_2}$ at room temperature under 350 nm of excitation are readily assigned. Four structured narrow visible emission bands at 480, 545, 580, and 620 nm of Tb^{3+} are assigned to an electronic transitions $^5D_4 \rightarrow {}^7F_J$

dx.doi.org/10.1021/ic2004672 |*Inorg. Chem.* 2011, 50, 5517–5525

Table 1. Crystal Data and Structure Refinement Parameters for GdL_1 and TbL^1

compound	GdL_1	TbL_1
empirical formula	$Gd_2C_{46}H_{66}N_{10}O_{18}$	$Tb_2C_{46}H_{66}N_{10}O_{18}$
mw	1685.86	1689.22
cryst color, habit	colorless, block	colorless, block
cryst size/mm	0.01 × 0.04 × 0.2	0.05 × 0.06 × 0.48
cryst syst	orthorhombic	orthorhombic
space group	P_{bca} (no.61)	*Pbca* (no.61)
unit cell dimesions	a = 19.1214(14) Å; b = 14.4071(10) Å; c = 24.2249(17) Å; α, β, γ = 90.000(0)°	a = 19.1573(10) Å; b = 14.4252(8) Å; c = 24.4261(13) Å; α, β, γ = 90.000(0)°
U/Å^3	6673.6(8)	6750.1(6)
Z	4	4
D_{calc}/g cm^{-3}	1.624	1.662
F(000)	3336	3464
Diffractometer	Bruker SMART 1000 CCD	Bruker SMART 1000 CCD
Radiation	Mo Kα (λ = 0.71073 Å)	Mo Kα (λ = 0.71073 Å)
μ(Mo Kα)/cm^{-1}	2.07	2.18
temp/K	296	299
reflns collected	46098	46166
unique reflns	8851	43834
observed reflns [I > 2σ(I)]	4821	5607
refinement method	full-matrix least-squares	full-matrix least-squares
weighting scheme	$w = 1/[\sigma^2(F_o^2) + (0.0545P)^2 + 28.4207P]$, where $P = (F_o^2 + 2F_c^2)/3$	$w = 1/[\sigma^2(F_o^2) + (0.0621P)^2 + 23.2475P]$, where $P = (F_o^2 + 2F_c^2)/3$
R	0.043	0.04
R_w	0.147	0.129
goodness of fit	1.08	1.05
maximum Δ/σ	0.001	0.002
no. of params	434	380
residual electron density/e Å^{-3}	1.44 to −0.90	1.31 to −0.79

Table 2. Selected Bonds for the Crystal Structures of GdL_1 and TbL_1

selected bond	bond length	selected bond	bond length
Gd1−O1	2.385 (6)	Tb1−O1	2.376 (4)
Gd1−O3	2.321 (5)	Tb1−O3	2.308 (4)
Gd1−O5	2.356 (5)	Tb1−O5	2.351 (4)
Gd1−O7	2.436 (4)	Tb1−O7	2.426 (4)
Gd1−O8	2.427 (5)	Tb1−O8	2.432 (4)
Gd1−N1	2.674 (5)	Tb1−N1	2.670 (4)
Gd1−N2	2.631 (6)	Tb1−N2	2.635 (4)
Gd1−N3	2.659 (6)	Tb1−N3	2.644 (5)
Gd1−N4	2.685 (6)	Tb1−N4	2.675 (4)

(J = 6, 5, 4, 3), whereas bands at 694, 620, 650, and 700 nm of Eu^{3+} complexes EuL_1 and EuL_2 correspond to $^5D_0 \rightarrow {}^7F_J$ (J = 1, 2, 3, 4).

As expected, the emission spectra of TbL_1 and TbL_2 are very similar and so are the spectra of EuL_1 and EuL_2. A high and similar intensity for the ΔJ = 0 transitions that belonged to the low axial symmetry (C_2) of europium ions in EuL_1 and EuL_2 was recorded (Figure 3a). Moreover, the ratio of relative intensity of the hypersensitive electric dipole allowed ΔJ = 2 transition compared to the ΔJ = 1 magnetic-dipole transition was constant for EuL_1 and EuL_2. The overall shapes of the emission spectra of both Eu complexes and Tb complexes are similar, suggesting a similar chemical environment of the metal ions. The emission quantum yields of Eu/Tb complexes varied; this reflects different sensitization efficiency of terbium or europium emissions between the two ligands (L_1 and L_2). LnL_2 (Ln = Eu and Tb) showed stronger emission intensities and higher quantum yield than LnL_1, which is expected because of the more efficient pathway and stronger absorption properties of LnL_2. The absorption coefficients of the two lanthanide series are similar, and the energy levels of the triplet states of the two bridged chromophores in these two series of lanthanide complexes were critical. The triplet states of these two lanthanide systems with two ligands were determined with the analogue gadolinium complexes GdL_1 and GdL_2 at cold temperatures. The slight differences of the two complexes' structures affect their optical properties. LnL_1 has a linear structure and methoxy group attached to the aromatic ring; this will directly affect the triplet state energy level and, in return, will affect the overlapping with the lanthanide energy level. Figure 3 shows that a LnL_2 triplet state energy state has a better overlap with those of the lanthanides, hence giving a stronger emission. In Figure 2, we can assume that the coordination environments of gadolinium and terbium/europium analogue complexes are similar. The lowest energy level of Gd^{3+} ($^6P_{7/2}$) is much higher than the energy levels of the ligands; therefore, it is assumed that there is no energy transfer between the ligand and metal.[37] In the case of Gd complexes, strong blue emission was recorded from their

dx.doi.org/10.1021/ic2004672 |*Inorg. Chem.* 2011, 50, 5517–5525

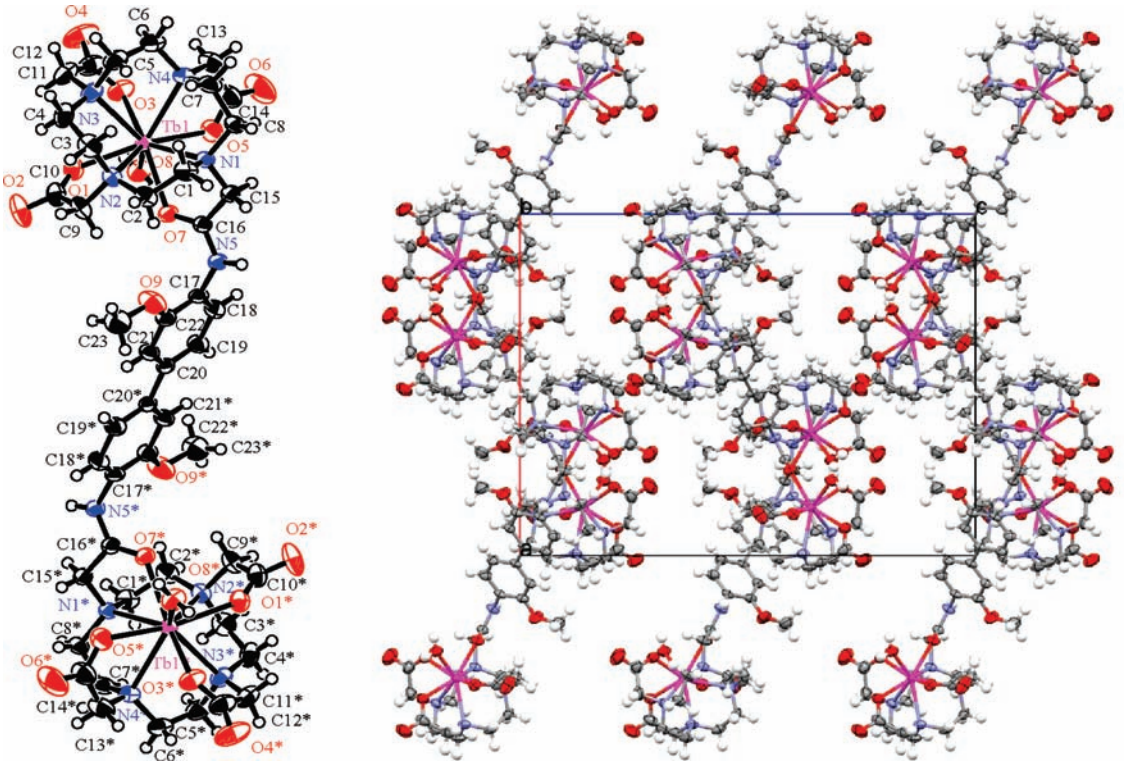

Figure 2. (Left) The molecular structure of [Tb$\mathbf{L}_2$] for atom labeling and (right) the cell-packing diagram of [Tb$\mathbf{L}_2$] without solvated water molecules and projected down the *b* axis.

Table 3. Photophysical Properties and IC_{50} Values of Lanthanide Complexes LnL_1−LnL_2 (Ln = Eu and Tb)

	$\varepsilon/M^{-1}\ cm^{-1}$	τ/ms[a]	ϕ	IC_{50}/mM
Eu$\mathbf{L}_1$	5230	1.05	0.04	3.1
Eu$\mathbf{L}_2$	5500	1.12	0.07	3.1
Tb$\mathbf{L}_1$	4980	1.51	0.08	2.9
Tb$\mathbf{L}_2$	5200	1.62	0.13	3.2

[a] Decay curve monitored at 545 nm ($^5D_0 \rightarrow {}^7F_2$, λ_{ex} = 350 nm) and at 620 nm ($^5D_4 \rightarrow {}^7F_5$, λ_{ex} = 350 nm) in DMSO.

ligands at ~400 nm at room temperature. Red-shifted phosphorescence emission bands in microseconds were observed in the two Gd complexes, and they are located at 455 nm (21 978 cm^{-1}) for Gd$\mathbf{L}_1$ and 440 nm (22 727 cm^{-1}) for Gd$\mathbf{L}_2$. The energy gap between the triplet state of the ligand and excited states of Tb/Eu in Ln$\mathbf{L}_2$ (>2000 cm^{-1}) is more suitable for energy transfer and antenna f−f emission. The phosphorescence of these Gd complexes was measured at low temperatures (77 K) in a glassy matrix of butyronitrile and acetonitrile, and the phosphorescence emission was assumed to be from the ligand's triplet state. The microsecond lifetime of the emission bands of the two gadolinium complexes in 77 K were further confirmed to be phosphorescence.

c. Photophysical Responses to Human Serum Albumin. Apart from showing a stronger antenna effect, Ln$\mathbf{L}_2$ also gave a responsive f−f luminescence enhancement toward HSA. Figure 4 shows that the shape of the emission spectrum, particularly the relative intensities of the bands, is affected owing to the hypersensitivity of the ΔJ = 2 transition (Figure 4). This alteration in spectroscopic signal may be due to the changes in the coordination environment of the europium ion after binding

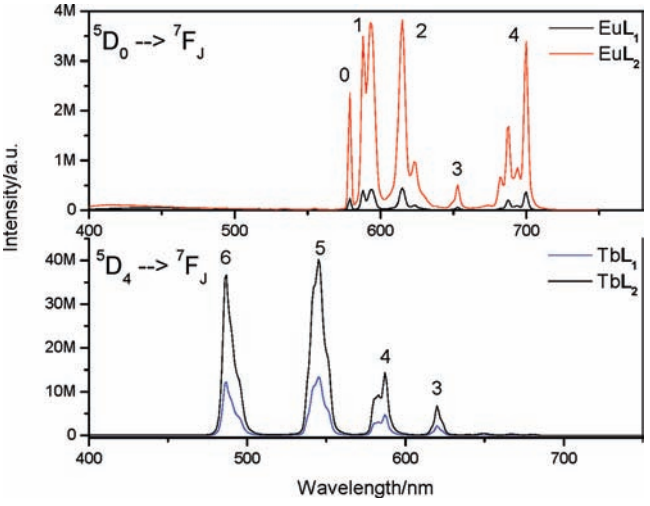

Figure 3. The emission spectra of Eu$\mathbf{L}_1$−Eu$\mathbf{L}_2$ (upper) and Tb$\mathbf{L}_1$−Tb$\mathbf{L}_2$ (lower) in DMSO (λ_{ex} = 350 nm, 30 μM complex).

with bulky HSA, and the hypersensitive emission can be used for the real-time detection of proteins. The ratio of $^5D_0 \rightarrow {}^7F_2$ transition to $^5D_0 \rightarrow {}^7F_1$ increased with the addition of HSA (Figures 4 and 5). Europium luminescence titrations were carried out in order to study the effect of the protein (HSA was first lyophilized and then added to the complex solution) using a simulated extra cellular anion mixture, with 0.7 mM HSA added to the background medium. The binding constant of Eu$\mathbf{L}_2$ to HSA was determined and is shown in Figure 5. The protein affinity of Eu$\mathbf{L}_2$ can be described by an apparent binding constant. Values for log K = 4.84 (±0.03) were calculated from

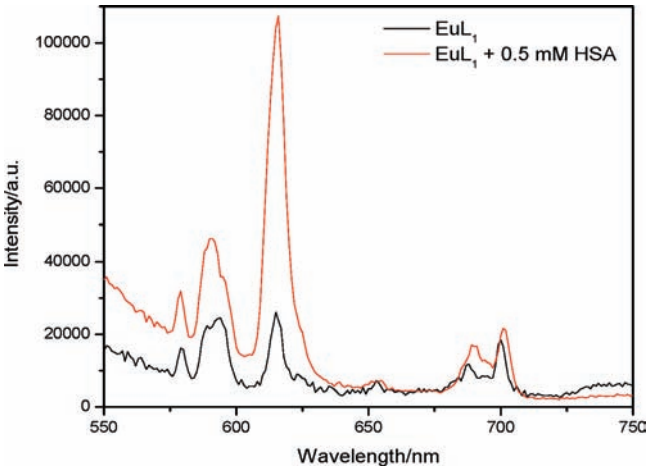

Figure 4. Responsive europium emission enhanced and ratio changes after 10 μM Eu$\mathbf{L_2}$ bound with 0.5 mM HSA in HEPES.

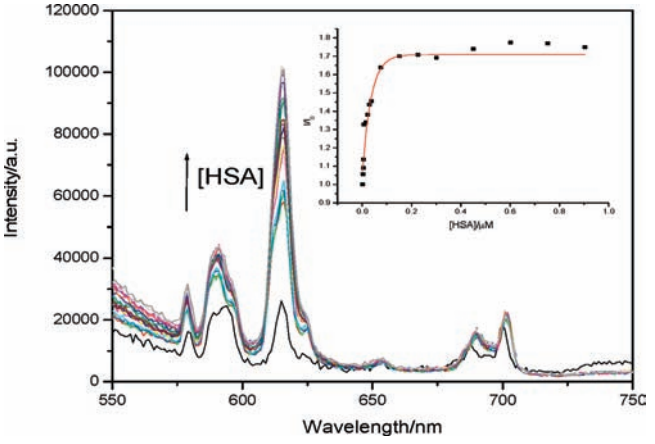

Figure 5. Variation of Eu emission spectrum for Eu$\mathbf{L_2}$ following addition of HSA (HEPES, pH 7.4, complex =10 μM, 298 K, λ_{ex} = 350 nm, 0.1 M NaCl). (Inset) Intensity ratio (615 nm) vs added HSA (0.5 μM to 1 mM) for deterring apparent binding constant.

the $^5D_0 \rightarrow {}^7F_2$ intensity versus [HSA] plot. Other titration experiments were carried out, and there were no emission enhancing/quenching effects in the europium emission of Eu$\mathbf{L_2}$ upon titration of small biological anions such as bicarbonate, phosphate, citrate, urates, and ascorbates (Figure S5, Supporting Information). To further characterize the protein affinity of Eu$\mathbf{L_2}$ with solid-phase protein quantitatively,[36] a decreasing amount of HSA (500−3.9 ng) was separated by SDS-polyacrylamide gel electrophoresis and analyzed using a fluorescence imager. As shown in Figure 6, an emissive gel image was obtained after staining HSA with Eu$\mathbf{L_2}$ for half an hour, and the amount of HSA detected in the gel was down to 3.9 ng/lane, suggesting that Eu$\mathbf{L_2}$ is a highly sensitive dye for protein detection in the presence of nonprotein interfering substances.

Tb$\mathbf{L_2}$ indeed showed enhancement with titration with HSA, but not as much as europium; less than 20% enhancement of f−f emission was observed. The protein affected the triplet state of the ligand and red-shifted the ligand and thus became more appropriate for the energy transfer to europium, rather than

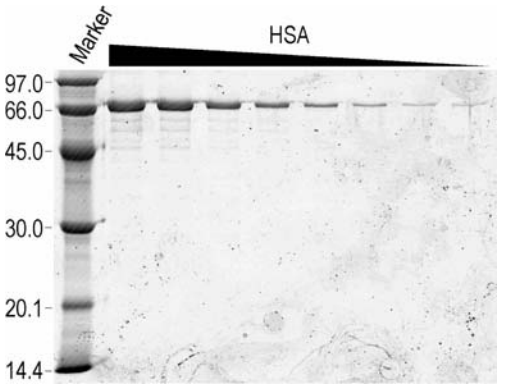

Figure 6. Emissive gel image. HSA in decreasing concentrations (500−3.9 ng) was loaded on the SDS-PAGE gel. The gel was fixed, stained with the dye for 30 min, and analyzed with Typhoon Trio Image (GE) with excitation and emission at 457 and ~620 nm, respectively.

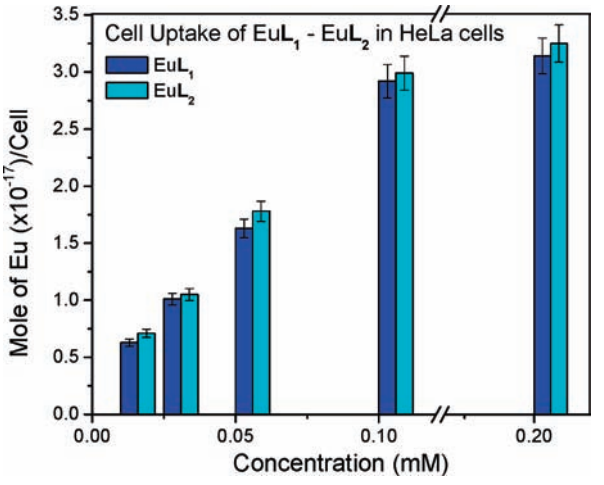

Figure 7. The cellular uptake of Eu$\mathbf{L_1}$−Eu$\mathbf{L_2}$ (incubation time = 6 h) in HeLa cell.

terbium, therefore causing a significant enhancement of the europium emission.

Ln$\mathbf{L_2}$ has a symmetrical bent geometric shape which is similar to that of BPA. Its bending structure might suggest that $\mathbf{L_2}$ had similar interactions with HSA compared with BPA, which binds to various biological molecules. Ln$\mathbf{L_1}$, which is a linear structure, did not show any enhancement of f−f luminescence when HSA was added.

d. *In Vitro* Studies. HeLa cells (Human Cervical Carcinoma Cell) were used to investigate the time-uptake profile and the localization profiles *in vitro* with the two europium complexes (Eu$\mathbf{L_1}$ and Eu$\mathbf{L_2}$; see Figure 7). A cellular-uptake experiment with carcinoma HeLa cells was performed to investigate the targeting ability of the complexes. The experiment was carried out in various concentrations of europium complexes Eu$\mathbf{L_1}$ and Eu$\mathbf{L_2}$ (0.01−0.2 mM) for 6 h. After incubation for 6 h, the cells were rinsed three times and harvested for cell counts. The europium concentrations in the cells were determined by ICP-MS, and the amount of europium per cell was calculated. Analysis of these two complexes treated with HeLa cells by ICP-MS showed that both complexes can effectively enter the cancer cells with the dependence of concentration for the level of cellular-uptake.

dx.doi.org/10.1021/ic2004672 |*Inorg. Chem.* 2011, 50, 5517–5525

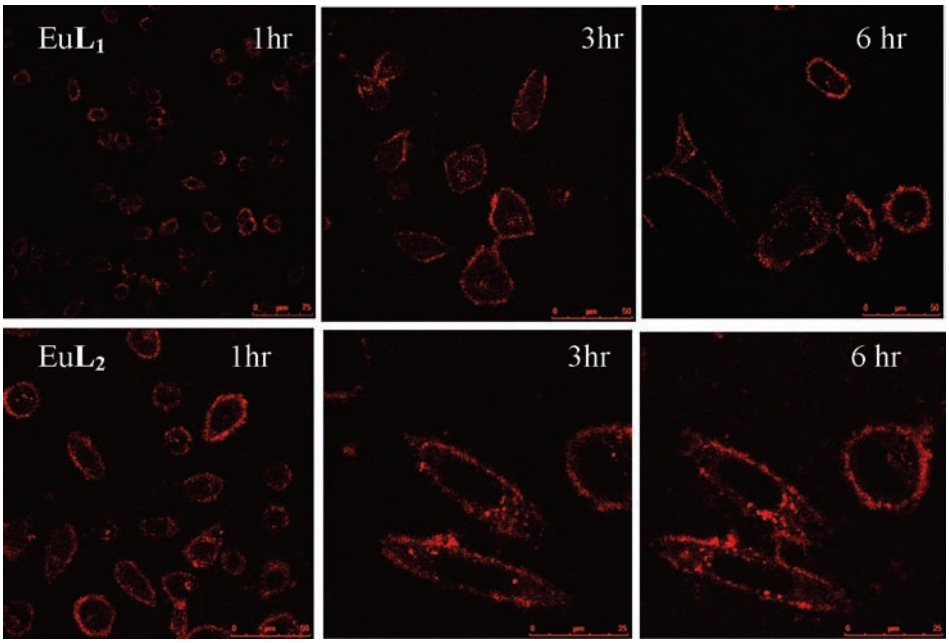

Figure 8. The *in vitro* imaging of complex Eu$\mathbf{L_1}$ and Eu$\mathbf{L_2}$ in HeLa cells for 1, 3, and 6 h (λ_{ex} = 380 nm, BP filter = 550−650 nm, 10 μM complex).

We extended the application of these two europium complexes as long-lived luminescent probes for *in vitro* imaging. The 5 μM europium complexes (1:99 = DMSO/H_2O) were incubated for different durations (1, 3, 4 and 6 h) in HeLa cells (and their in vitro images were also recorded). After 3 h of incubation, only the HeLa cells with Eu$\mathbf{L_2}$ showed red emission in cytoplasm upon UV excitation (Figure 8), and no significant cell death was observed. After another 3 h, over 90% of the cells showed red luminescence in the cytoplasm with Eu$\mathbf{L_2}$. A similar observation was made in complex Eu$\mathbf{L_1}$, but the luminescence observed was inside the cytoplasm after another 3 h of incubation time. There was no evidence of cytotoxicity in the HeLa cells that had been exposed to the europium complexes Eu$\mathbf{L_1}$ or Eu$\mathbf{L_2}$ for 24 h (Figure S5, Supporting Information) at 50 μM. MTT assays on these cells exposed to 50 μM europium complexes for prolonged periods revealed no significant decrease in the number of viable cells. In addition, the nontoxic IC_{50} values of the complexes in HeLa cells were found to be ~3 mM. It is worth noting that the lanthanide complex was mostly distributed inside the cytoplasm. All of these data indicate that these two complexes could be developed into a time-resolved turn-on probe for bioimaging.

CONCLUSION

Two series of dimeric DO3A lanthanide complexes were synthesized and bridged with two different amide chromophores. The molecular structures of rare dimeric lanthanide DO3A complexes (Gd$\mathbf{L_1}$ and Tb$\mathbf{L_1}$) have been reported. Ln$\mathbf{L_2}$ which is bridged with bisphenyl demonstrated adequate f−f emission quantum yield. Eu$\mathbf{L_2}$ also showed selectivity toward HSA enhancing f−f emission and changing in real-time hypersensitive f−f emission. No significant cytotoxicity (IC_{50} > 3 mM) and a fast uptake of lanthanide complexes were recorded in HeLa cells for both series. *In vitro* imaging of HeLa cells with Eu$\mathbf{L_1}$ and Eu$\mathbf{L_2}$ was performed, and strong red f−f emission was observed.

ASSOCIATED CONTENT

Supporting Information. Experimental details of syntheses, ESI-MS spectra of complexes, UV−vis absorption and emission spectra, MTT assay, and crystal data for Gd$\mathbf{L_1}$ and Tb$\mathbf{L_1}$. This material is available free of charge via the Internet at http://pubs.acs.org.

ASSOCIATED CONTENT

Supporting Information. The mass spectra of Eu$\mathbf{L_2}$, absorption spectra of complexes Eu$\mathbf{L_1}$ and Eu$\mathbf{L_2}$, fluorescence and phosphorescence of Gd$\mathbf{L_1}$−Gd$\mathbf{L_2}$ complexes, titration of Eu emission spectrum for Eu$\mathbf{L_2}$, and MTT assay results of lanthanide complexes Eu$\mathbf{L_1}$−Eu$\mathbf{L_2}$ and Tb$\mathbf{L_1}$−Tb$\mathbf{L_2}$. This material is available free of charge via the Internet at http://pubs.acs.org

AUTHOR INFORMATION

Corresponding Author
*Tel.: (852) 3400 8789. E-mail:bcwtwong@polyu.edu.hk.

ACKNOWLEDGMENT

This work was funded by grants from The Hong Kong Research Grants Council (PolyU 503510P) and The Hong Kong Polytechnic University (1BD07), Hong Kong Chinese University, and Hong Kong Baptist University (FRG 1/10-11/037). This work was also supported by the Area of Excellence Scheme of the University of Grants Committee (Hong Kong).

REFERENCES

(1) Tanner, P. A.; Duan, C.-K. *Coord. Chem. Rev.* **2010**, *254*, 3026–3029.
(2) Binnemans, K. *Chem. Rev.* **2009**, *109*, 4283–4373.
(3) Law, G.-L.; Wong, K.-L.; Szeto, L.; Lau, K.-K.; Tanner, P. A.; Wong, W.-T. *J. Mater. Chem.* **2010**, *20*, 4074–4079.

(4) Zucchi, G.; Jeon, T.; Tondelier, D.; Aldakov, D.; Thuéry, P.; Ephritikhine, M.; Geffroy, B. *J. Mater. Chem.* **2010**, *20*, 2114–2120.
(5) Law, G.-L.; Wong, K.-L.; Chen, Z.-H.; Tam, H.-L.; Cheah, K.-W.; Wong, W.-T. *Inorg. Chem.* **2009**, *48*, 10492–10494.
(6) Kido, J.; Okamoto, Y. *Chem. Rev.* **2002**, *102*, 2357–2368.
(7) Karhunen, U.; Jaakkola, L.; Wang, Q.; Lamminmaki, U.; Soukka, T. *Anal. Chem.* **2010**, *82*, 751–754.
(8) Gunawan, P.; Xu, R. *J. Phys. Chem. C* **2009**, *113*, 17206–17214.
(9) Poudret, L.; Prior, T. J.; McIntyre, L. J.; Fogg, A. M. *Chem. Mater.* **2008**, *20*, 7447–7453.
(10) Wong, K.-L.; Law, G.-L.; Yang, Y.-Y.; Wong, W.-T. *Adv. Mater.* **2006**, *18*, 1051–1054.
(11) Tsukube, H.; Shinoda, S. *Chem. Rev.* **2002**, *102*, 2389–2404.
(12) Bünzli, J. C. G. *Chem. Rev.* **2010**, *110*, 2729–2755.
(13) Berezin, M. Y.; Achilefu, S. *Chem. Rev.* **2010**, *110*, 2641–2684.
(14) Law, G.-L.; Wong, K.-L.; Man, W.-Y. C.; Tsao, S-.W.; Wong, W.-T. *J. Biophotonics* **2009**, *2*, 718–724.
(15) Montgonery, C. P.; Murray, B. S.; News, E. J.; Pal, R.; Parker, D. *Acc. Chem. Res.* **2009**, *42*, 925–937.
(16) New, E. J.; Parker, D.; Smith, D. G.; Walton, J. W. *Curr. Opin. Chem. Bio.* **2010**, *14*, 238–246.
(17) Eliseeva, S. V.; Aubv̈ck, G.; van Mourik, F.; Cannizzo, A.; Song, B.; Deiters, E.; Chauvin, A.-S.; Chergui, M.; Bv̈nzli, J. C. G. *J. Phys. Chem. B.* **2010**, *114*, 2932–2937.
(18) Picot, A.; D'Aléo, A.; Baldeck, P. L.; Grichine, A.; Duperray, A.; Andraud, C.; Maury, O. *J. Am. Chem. Soc.* **2008**, *130*, 1532–1533.
(19) Law, G.-L.; Wong, K.-L.; Kwok, W.-M.; Tanner, P. A.; Wong, W.-T. *J. Phys. Chem. B* **2007**, *111*, 10858–10861.
(20) Pälsson, L.-O.; Pal, R.; Murray, B. S.; Parker., D.; Beeby, A. *Dalton Trans.* **2007**, 5726–5734.
(21) Wong, K.-L.; Kwok, W,-M.; Wong, W.-T.; Phillips, D. L.; Cheah, K.-W. *Angew. Chem., Int. Ed.* **2004**, *43*, 4659–4662.
(22) Placidi, M. P.; Villaraza, A.-J. L.; Natrajan, L.-S.; Sykes, D.; Kenwright, A. M.; Faulkner, S. J. *Am. Chem. Soc.* **2009**, *131*, 9916–9917.
(23) Kielar, F.; Congreve, A.; Law, G.-L.; New, E. J.; Parker, D.; Wong, K.-L.; Prados, P.; de Mendoza, J. *Chem. Commun.* **2008**, *21*, 2435–2437.
(24) Li, C.; Li, Y.-X.; Law, G.-L.; Man, K.; Wong, W.-T.; Lei, H. *Bioconjugate Chem.* **2006**, *17*, 571–574.
(25) Rudovsk, J.; Botta, M.; Herman, P.; Koridze, A.; Amine, S. *Dalton Trans.* **2006**, *19*, 2323–2333.
(26) Pope, S. J. A.; Kenwright, A. M.; Boote, V. A.; Faulkner, S. *Dalton Trans.* **2003**, *19*, 3780–3784.
(27) Gunnlaugsson, T.; Harte, A. J.; Leonard, J. P.; Nieuwenhuyzen, M. *Chem. Commun.* **2002**, *18*, 2134–2135.
(28) Shiraishi, Y.; Farabayashi, Y.; Nishimura, G.; Hirai, T. J. *Luminescence* **2007**, *127*, 623–632.
(29) Elbahir, M.; Scopelliti, R.; Bunzli, J-C. G.; Piguet, C. *J. Am. Chem. Soc.* **1999**, *121*, 9326–9342.
(30) Harte, A. J.; Jensen, P.; Plush, S. E.; Kruger, P. E.; Gunnlaugsson, T. *Inorg. Chem.* **2006**, *45*, 9465–9474.
(31) Xie, X.; Wang, X.; Xu, X.; Sun, H.; Chen, X. *Chemosphere* **2010**, *80*, 1075–1080.
(32) Okada, K.; Hashimoto, S.; Imakoka, S. *JHS* **2010**, *56*, 1–13.
(33) Matsushima, A.; Kakuta, Y.; Teramoto, T.; Koshiba, T.; Liu, X.; Okada, H.; Tokunaga, T.; Kawabata, S.; Kimura, M.; Shimohigashi, Y. *J. Biochem.* **2007**, *142*, 517–524.
(34) Kahn, O. *Acc. Chem. Res.* **2000**, *33*, 647–657.
(35) Nishibu, T.; Hirayasu, K.; Tanaka, T.; Takeda, Y.; Kobayashi, Y. *Anal. Biochem.* **2003**, *319*, 88–95.
(36) Wilson, A. P., *Cytotoxicity and Viability Assays in Animal Cell Culture: A Practical Approach*, 3rd ed. (ed.Masters, J. R. W.) Oxford University Press: Oxford, 1, (2000)
(37) Law, G.-L.; Wong, K.-L.; Lau, K.-K.; Tam, H.-L.; Cheah, K.-W.; Wong, W.-T. *Eur. J. Inorg. Chem.* **2007**, 5419–5425.